8546 *Biochemistry* **2010,** *49,* 8546–8553
DOI: 10.1021/bi1006783

BIOCHEMISTRY
including biophysical chemistry & molecular biology
Article

Enzymatic Interconversion of Ammonia and Nitrite: The Right Tool for the Job[†]

Joshua Kostera, Jennifer McGarry, and A. Andrew Pacheco*

Department of Chemistry and Biochemistry, University of Wisconsin, Milwaukee, Wisconsin 53211

Received May 1, 2010; Revised Manuscript Received August 6, 2010

ABSTRACT: Hydroxylamine oxidoreductase (HAO) from *Nitrosomonas europaea* normally catalyzes oxidation of NH_2OH to NO_2^-. This paper reports experiments in which HAO was thermodynamically poised to catalyze reduction of NO_2^- to NH_4^+. HAO was found to catalyze the reduction of NO_2^- by methyl viologen monocation radical (MV_{red}), displaying a hyperbolic dependence on NO_2^- concentration, with a k_{cat1} of $6.8 \pm 0.3\ s^{-1}$ and a K_{m1} of 7.6 ± 0.9 mM. HAO also catalyzed the reduction of NH_2OH by MV_{red}, with a hyperbolic dependence on NH_2OH concentration, and a k_{cat2} of $245 \pm 3\ s^{-1}$ and a K_{m2} of 6.8 ± 0.2 mM (k_{cat1} and k_{cat2} reflect the maximum number of electrons transferred from MV_{red} per second). We had previously demonstrated that HAO catalyzes the reduction of NO by MV_{red} to yield first NH_2OH and then NH_4^+. Thus, overall, HAO is seen to act like a cytochrome *c* nitrite reductase, which catalyzes the six-electron reduction of NO_2^- to NH_4^+ by MV_{red}. In the presence of $Ru(NH_3)^{2+}$ (Ru^{II}) and $Ru(NH_3)^{3+}$ (Ru^{III}) at ratios exceeding 200:1, HAO exhibited no detectable $Ru^{II}-NO_2^-$ oxidoreductase activity, though such activity is thermodynamically favored. On the other hand, HAO could still catalyze the oxidation of NH_2OH to NO by Ru^{III} under these conditions. The oxidative process exhibited a hyperbolic dependence on NH_2OH concentration, with a k_{cat3} of $98 \pm 3\ s^{-1}$ and a K_{m3} of $5.2 \pm 0.8\ \mu M$. Finally, HAO was found not to catalyze the disproportionation of NH_2OH, despite the thermodynamic favorability of such a process, and the apparent opportunity presented by the HAO structure. Mechanisms are proposed to explain all the kinetic data.

In the process of extracting energy from the environment via respiration, a variety of bacteria interconvert ammonia and nitrite. Ammonia-oxidizing bacteria (AOB)[1] such as *Nitrosomonas europaea* use ammonia almost exclusively as an electron donor in respiration and oxidize it to nitrite (Figure 1) (*1*). Conversely, a subclass of bacteria that use nitrite as a terminal electron acceptor in the absence of oxygen reduce the nitrite to ammonia in a process known as nitrite ammonification (Figure 1) (*2*). In AOB, the enzyme hydroxylamine oxidoreductase (HAO) typically catalyzes the four-electron oxidation of hydroxylamine to nitrite, which is the second step in ammonia-dependent respiration. HAO is structurally quite similar to the enzyme cytochrome *c* nitrite reductase (ccNiR), which catalyzes the six-electron reduction of nitrite to ammonia, in the anaerobic bacteria that use the nitrite ammonification pathway. In many respects, HAO and ccNiR perform opposing jobs. Even though HAO oxidizes hydroxylamine to nitrite rather than ammonia, the two enzymes probably go through many comparable reactive intermediates (*3*). Given the structural similarities between HAO and ccNiR, and the fact that they probably catalyze similar reactions in opposing directions, our research group is very interested in understanding whether the enzymes are optimized to preferentially operate in one direction or the other and, if so, how. In a previous paper, we described how HAO could catalyze the reduction of NO and NH_2OH by methyl viologen monocation radical (MV_{red}) (*3*). Herein, we show that HAO also catalyzes the reduction of NO_2^- by MV_{red} and explore the limits of its reductase capacity.

Of the two enzymes ccNiR and HAO, the latter is more complex. This enzyme is a homotrimer that contains eight hemes per monomer. The active sites are three unique hemes termed P_{460}s, which have a vacant site where NH_2OH molecules can bind and react. The 21 remaining hemes are typical six-coordinate *c* hemes that serve to efficiently move electrons away from the active sites (*4*−*6*). CcNiR is only slightly less complex than HAO. Crystal structures have been reported for ccNIRs from many different bacteria, and all show enzymes that are homodimers, with molecular masses ranging from 52 to 65 kDa/monomer, and containing a total of 10 hemes (five per monomer) (*7*−*10*). Eight of the 10 hemes are six-coordinate, with histidines providing axial ligation. The two active site hemes (one per monomer) have the unusual ligand lysine at one axial position, leaving the other position open to accept the substrate NO_2^- (*7*−*10*).

At this point, it is important to consider the energetics of ammonia−nitrite interconversion from the point of view of the organisms involved in the process. Nitrite reducers are using NO_2^- as an electron acceptor under anaerobic conditions. These are the conditions under which ccNiR operates, and a Frost diagram for nitrogen at pH 7 (*11*, *12*) (Figure 2a) provides a helpful portrayal of the associated energetics. As is conventional, the Frost diagram in Figure 2a shows the energy of each nitrogen species relative to the normal hydrogen electrode (NHE), the H^+/H_2 couple at pH 0 and 1 bar of H_2 gas. The NHE couple represents fairly reducing conditions from a physiological standpoint, reasonably similar to the conditions encountered by the

[†]This publication was made possible by support from the National Science Foundation (Grant MCB-0843459) and from the University of Wisconsin—Milwaukee's Research Growth Initiative (101X076).

*To whom correspondence should be addressed. Phone: (414) 229-4413. Fax: (414) 229-5530. E-mail: apacheco@uwm.ed.

[1]Abbreviations: AOB, ammonia-oxidizing bacteria; HAO, hydroxylamine oxidase; ccNiR, cytochrome *c* nitrite reductase; α-KG, α-ketoglutarate; GDH, glutamate dehydrogenase; MV_{red}, one-electron-reduced methyl viologen monocation radical; MV_{ox}, methyl viologen fully oxidized dication; Cat, catalase; CatNO, nitrosylated catalase; C_{554}, cytochrome c_{554}; SVD, singular-value decomposition; DEANO, 1-(*N*,*N*-diethylamino)diazen-1-ium 1,2-diolate.

 Published on Web 09/02/2010

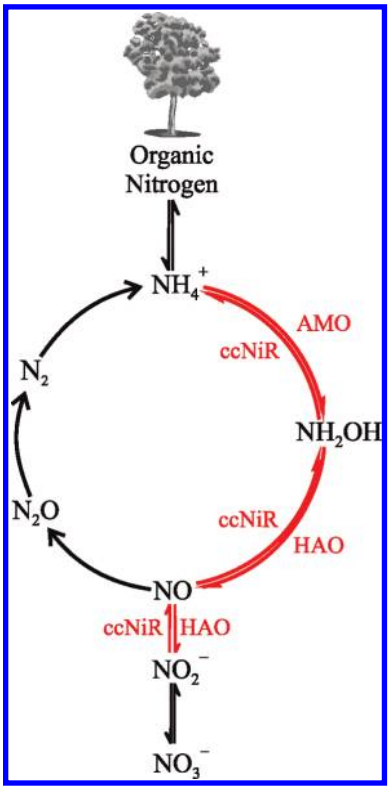

FIGURE 1: Biological nitrogen cycle with ammonia−nitrite interconversion highlighted in red. Oxidation of ammonia to nitrite by ammonia-oxidizing bacteria (AOB) occurs in two steps. Oxidation of ammonia to hydroxylamine is catalyzed by ammonia monooxygenase (AMO), and oxidation of hydroxylamine to nitrite is catalyzed by hydroxylamine oxidoreductase (HAO). Nitrite reduction by nitrite-ammonifying bacteria is catalyzed by the single enzyme cytochrome *c* nitrite reductase (ccNiR, also termed nrfA by some investigators).

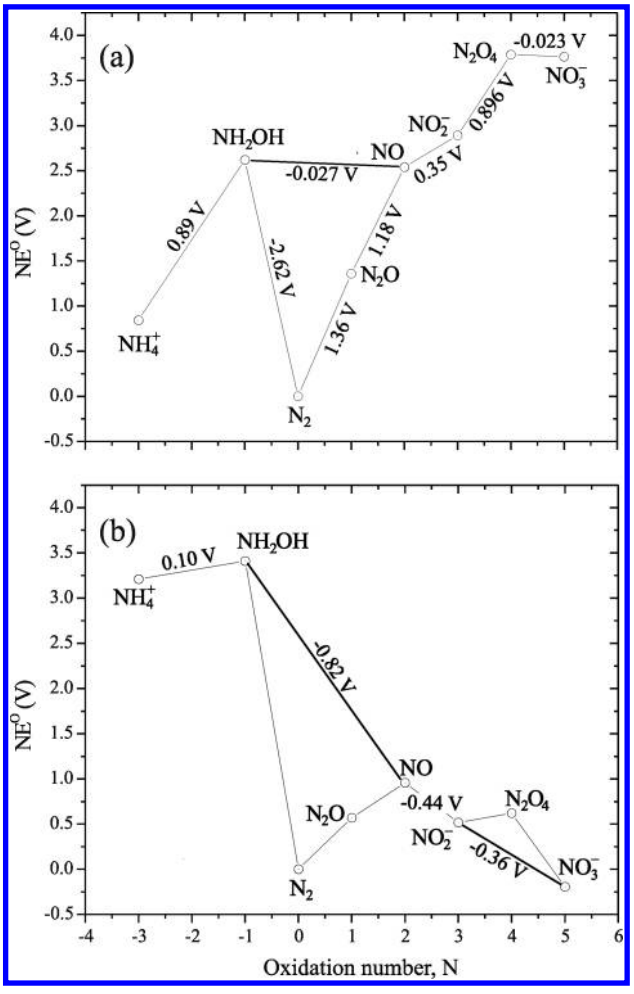

FIGURE 2: (a) Frost diagram for nitrogen at pH 7.0. (b) Frost-like diagram for nitrogen, in which the energy of each nitrogen species is given relative to the O_2/H_2O couple (at pH 7) instead of the NHE.

nitrite reducers. Under these conditions, it is clear that NH_4^+ is the thermodynamically most stable monomeric nitrogen species, while N_2 is the most stable nitrogen species overall. Hence, it is easy to see from Figure 2a how nitrite reducers extract energy from reduction of NO_2^- to NH_4^+.

In contrast to nitrite reducers, ammonia oxidizers are using NH_4^+ as an electron source and O_2 as the electron acceptor. The conventional Frost diagram of Figure 2a is a poor portrayal of these energetics, but the situation is easily remedied by replacing Figure 2a with a "Frost-like" diagram (Figure 2b), in which the energy of each nitrogen species is given relative to the O_2/H_2O couple (at pH 7) instead of NHE. In Figure 2b, NH_4^+ and NH_2OH are the highest-energy monomeric nitrogen species in the diagram, whereas NO_2^- and NO_3^- are the most thermodynamically stable. Thus, it is easy to visualize from Figure 2b how ammonia oxidizers extract energy from oxidation of NH_4^+ to NO_2^-.

If the Frost diagrams of Figure 2 make it easy to see how nitrite reducers and ammonia oxidizers extract energy from the environment, they also show how easily the energetically preferred direction of ammonia−nitrite interconversion can be reversed under physiologically relevant conditions. It is this observation that sparked our interest in the extent to which HAO and ccNiR can be made to operate in their nonphysiological directions. In this paper, we focus on experiments in which HAO is run in reverse. We first show that, under sufficiently reducing conditions, HAO can in fact be turned into a "ccNiR", which can reduce NO_2^-, NO, and NH_2OH to NH_4^+. Next we present the results of experiments in which the kinetics of reduction of NH_2OH by HAO were analyzed as a function of the reduction potential at which the reaction solution was buffered. Taken together, our combined results reveal how HAO is cleverly optimized to kinetically favor oxidation of hydroxylamine under physiologically relevant conditions, even when reduction to ammonia is the thermodynamically favorable direction.

MATERIALS AND METHODS

Materials. HAO was purified as described in ref *13*, and cytochrome c_{554} (C_{554}) was purified by a slight modification of a method previously described by Arciero et al. (*14*). Methyl viologen dichloride, sodium nitrite, hexaammineruthenium(II) chloride, and hexaammineruthenium(III) chloride were obtained from Acros; sodium dithionite was from Aldrich, and hydroxylamine hydrochloride was from Fisher. Catalase from bovine liver was obtained from Sigma (C3155), as were NADH disodium salt (catalog number N8129), ketoglutaric acid disodium salt (K3752), and L-glutamate dehydrogenase from bovine liver (catalog number G2626). In experiments involving methyl viologen, the total concentration of this species was kept constant at 300 μM. The ratio of one-electron-reduced methyl viologen monocation radical (MV_{red}) to fully oxidized dication (MV_{ox}) was then adjusted via addition of an appropriate amount of sodium dithionite. The concentration of MV_{red} was typically ≤25% of the total methyl viologen concentration. All experiments were

performed in solutions buffered with phosphate (μ = 50 mM, pH 7.4), and all solutions were prepared and manipulated in a nitrogen-filled glovebox. Stock solutions were prepared daily and stored in a refrigerator at 4 °C until they were needed. Hydroxylamine hydrochloride stock solutions were prepared in nanopure water; all other stock solutions were made up in phosphate buffer (μ = 50 mM, pH 7.4).

Data Collection and Analysis. UV−vis spectra, both for routine characterization and for the kinetic experiments, were recorded using a Cary 50 spectrophotometer (Varian) that was installed in the glovebox. Data were analyzed using the commercially available software packages Microcal Origin version 6.0 (Microcal Software, Inc.) and Mathcad 13 (Mathsoft Engineering and Education, Inc.). Time-resolved spectra obtained using the Cary 50 spectrophotometer were first subjected to singular-value decomposition (SVD) to determine the number of colored species and to decrease the noise in the absorbance matrices (*15*). A matrix form of Beer's law (eq 1) was then used to calculate the concentrations of all species in solution as a function of time (*15*, *16*). In Eq 1,

$$\mathbf{C} = (1/l)(\mathbf{A})\cdot\boldsymbol{\varepsilon}^{\mathbf{T}}\cdot(\boldsymbol{\varepsilon}\cdot\boldsymbol{\varepsilon}^{\mathbf{T}})^{-1} \quad (1)$$

A is the SVD-processed absorbance matrix, in which each row corresponds to a spectrum and each column to a time trace at a fixed wavelength; $\boldsymbol{\varepsilon}$ is the matrix of extinction coefficients, in which each row corresponds to a unique species and each column to a wavelength; **C** is the matrix of concentrations, in which each column corresponds to a unique species and each row to a specific time; and l is a scalar representing the path length. The extinction coefficient difference spectra required in eq 1, as well as absolute extinction coefficient spectra used to calculate species concentrations in the cuvettes prior to reaction, were obtained as follows. The extinction coefficient spectra for MV_{ox}, MV_{red}, and HAO at various stages of reduction were obtained as described in ref *3*. The extinction coefficient for Cat is 1.2×10^5 M^{-1} cm^{-1} at 403 nm (*17*), and this value was used to obtain the concentration of a solution of Cat, which in turn was used to calculate the complete $\boldsymbol{\varepsilon}$ value spectrum for the enzyme. The Cat was then fully nitrosylated via addition of a large excess (~340 μM) of 1-(*N*,*N*-diethylamino)diazen-1-ium 1,2-diolate (DEANO), which decomposes to yield NO in situ (*18*, *19*), and the $\boldsymbol{\varepsilon}$ value spectrum for CatNO was obtained. A solution of C_{554} was titrated with Ti(III) citrate (*20*) to generate spectra at various stages of reduction. The concentration of the fully reduced C_{554} was obtained from the known extinction coefficient at 554 nm (2.46×10^4 M^{-1} cm^{-1}) (*21*), and this value was used to obtain the complete $\boldsymbol{\varepsilon}$ value spectrum for the reduced protein. After correction for dilution by added reductant, $\boldsymbol{\varepsilon}$ value spectra were generated for all the stages of reduction and stored in an electronic "lookup table". A Mathcad routine could then be used to determine the C_{554} concentration from the spectrum of any solution containing the protein, regardless of the protein's oxidation state. The $\boldsymbol{\varepsilon}$ value spectrum of reduced nitrosylated C_{554} was obtained by adding excess DEANO to the reduced protein, in a procedure analogous to that described above for Cat.

RESULTS

ccNiR Activity of HAO. HAO was found to catalyze the reduction of NO_2^- by MV_{red}. Figure 3 shows how the initial rate (V_0) of MV_{red} oxidation depends on the concentration of NO_2^-. The experimental data are fitted to a rectangular hyperbola

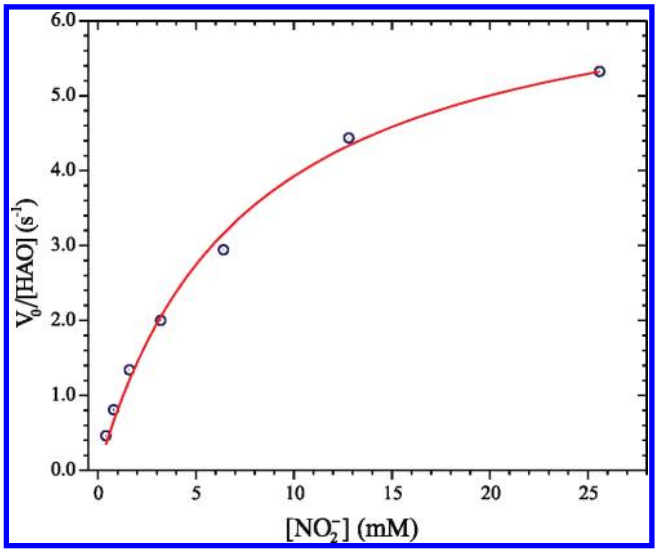

FIGURE 3: Initial rates of HAO-catalyzed MV_{red} oxidation by NO_2^- ($V_0 = -d[MV_{red}]/dt$ at time zero), as a function of $[NO_2^-]_0$; V_0/[HAO] is plotted on the abscissa to allow for variation of [HAO] between experiments. The red curve is the least-squares fit to eq 2; the values of the fit parameters, k_{cat1} and K_{m1}, are listed in Table 1.

(eq 2), in which k_{cat1} = 6.8 ± 0.3 s^{-1} and K_{m1} = 7.6 ± 0.9 mM (a subscript 1 is added to k_{cat} and K_m to distinguish these parameters from others defined below).

$$V_0 = \frac{k_{cat}[HAO][NO_2^-]}{K_m + [NO_2^-]} \quad (2)$$

Note that, as defined here, k_{cat1} reflects the maximum number of electrons transferred from MV_{red} per second. A one-electron reduction of NO_2^- will yield NO, as shown in Figure 1. We previously demonstrated that HAO catalyzes the reduction of NO by MV_{red} to yield first NH_2OH and then NH_4^+ (*3*). Thus, overall, HAO is seen to act like a cytochrome *c* nitrite reductase (ccNiR), capable of catalyzing the net six-electron reduction of NO_2^- to NH_4^+.

Hydroxylamine Reductase Activity of HAO. When HAO is used to catalyze the reduction of NH_2OH to NH_4^+ by MV_{red}, the initial rate of MV_{red} oxidation once again exhibits a hyperbolic dependence on the substrate, this time NH_2OH (Figure 4). Least-squares fitting to the experimental data (red trace in Figure 4) yields the following parameters: k_{cat2} = 245 ± 3 s^{-1} (which again reflects the maximum number of electrons transferred from MV_{red} per second), and K_{m2} = 6.8 ± 0.2 mM. Though the K_{m1} and K_{m2} values are comparable, k_{cat2} is seen to be nearly 40 times greater than k_{cat1}. Table 1 summarizes the kinetic parameters obtained for the MV_{red}−NO_2^- and MV_{red}−NH_2OH oxidoreductase activities.

MV_{red} is a very powerful reducing agent, but Figure 2a shows that even a reducing agent with an E^0 around 0 mV should be thermodynamically able to reduce NO_2^-, NO, or NH_2OH to NH_4^+. For example, $Ru(NH_3)_6^{3+}$ has a standard reduction potential of −24 mV versus NHE at pH 7.4 (*22*), which gives a standard cell potential of 0.91 V for the reduction of NH_2OH by $Ru(NH_3)_6^{2+}$ (Scheme 1). In addition, we have found that both $Ru(NH_3)_6^{2+}$ and $Ru(NH_3)_6^{3+}$ can exchange electrons with HAO on the submillisecond time scale (*22*), so in principle, $Ru(NH_3)_6^{2+}$ should be an excellent electron donor for the facile reduction of NH_2OH.

We measured HAO's $Ru(NH_3)_6^{2+}$−NH_2OH oxidoreductase activity by monitoring spectral changes at the 263 nm absorbance maximum of $Ru(NH_3)_6^{2+}$ (data not shown) but saw no evidence of Ru^{II} oxidation. However, neither oxidation state of the hexaammine has very high absorbance in the UV−vis region, so this test is not very sensitive. Figure 5 shows the results of a more sensitive test, in which cytochrome c_{554} (C_{554}) was used as a convenient redox indicator [C_{554} is more often considered the most likely candidate for HAO's physiological electron acceptor (*23*), but for the purposes of this experiment, that fact is secondary]. C_{554} is a tetraheme, in which two of the hemes have E_1^0 and E_2^0 values of 47 mV, and the other two have an E_3^0 of −147 mV and an E_4^0 of −276 mV (*14*, *24*). The experiment was initiated via addition of NH_2OH to a test solution already containing $Ru(NH_3)_6^{2+}$, $Ru(NH_3)_6^{3+}$, HAO, and C_{554}. The concentrations of the reagents after NH_2OH addition were as follows: 235 μM $Ru(NH_3)_6^{2+}$, 1 μM $Ru(NH_3)_6^{3+}$, 10 nM HAO, 1.23 μM C_{554}, and 910 μM NH_2OH. Initially, the solution [Ru^{II}]:[Ru^{III}] ratio of 235 results in complete reduction of the two high-potential hemes of C_{554}, and ~90% reduction of heme 3. The extent of C_{554} reduction was readily verified via analysis of its strong heme absorption bands, which change noticeably with oxidation state (*14*). Any subsequent $Ru(NH_3)_6^{2+}$ oxidation by NH_2OH should have been immediately apparent in Figure 5 by the concomitant oxidation of the C_{554} hemes. Indeed, Ru^{II} oxidation at the rate predicted by k_{cat2} and K_{m2} (Table 1) for oxidation of MV_{red} would have resulted in complete oxidation of both $Ru(NH_3)_6^{2+}$ and all of the C_{554} hemes, during the 20 min that the reaction was monitored. Oxidation of the C_{554} hemes should in turn have given rise to the red difference spectrum in Figure 5. Changes in the UV−vis spectrum are indeed seen after the addition of NH_2OH (Figure 5), but they are not the changes expected to accompany C_{554} oxidation. Instead, these are the changes associated with nitrosylation of the ferrous five-coordinate C_{554} heme 2 (unpublished observations of M. D. Youngblut and A. A. Pacheco and ref *25*). This observation shows that even in the presence of a large excess of $Ru(NH_3)_6^{2+}$, HAO is actually catalyzing the oxidation of NH_2OH to NO by $Ru(NH_3)_6^{3+}$. The standard cell potential for this reaction is only 3 mV (Scheme 1), but subsequent trapping of the generated NO by C_{554} will make the reaction more favorable.

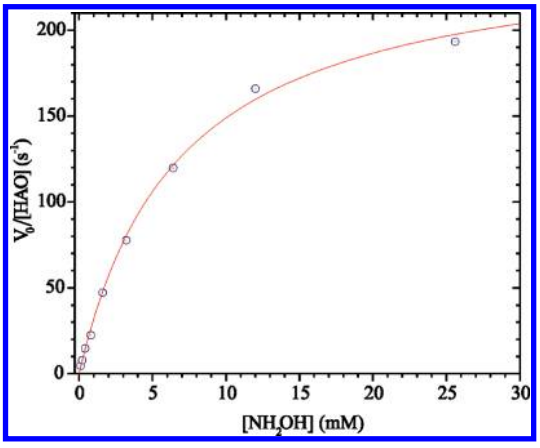

FIGURE 4: Initial rates of HAO-catalyzed MV_{red} oxidation by NH_2OH ($V_0 = -d[MV_{red}]/dt$ at time zero), as a function of $[NH_2OH]_0$; V_0/[HAO] is plotted on the abscissa to allow for variation of [HAO] between experiments. The red curve is the least-squares fit to eq 2; the values of the fit parameters, k_{cat2} and K_{m2}, are listed in Table 1.

HAO-Catalyzed Oxidation of Hydroxylamine to NO, in the Presence of Catalase as an NO Scavenger. To kinetically characterize HAO-catalyzed oxidation of NH_2OH to NO by $Ru(NH_3)_6^{3+}$, we used catalase (Cat) as an NO scavenger in place of C_{554}. Catalase has the advantages of being commercially available and of reacting much more rapidly with NO than C_{554} (M. D. Youngblut and A. A. Pacheco, unpublished observations). Thus, under our experimental conditions, the reaction of Cat with NO was much faster than the rate of production of NO from NH_2OH, so that the appearance of CatNO directly reflected the

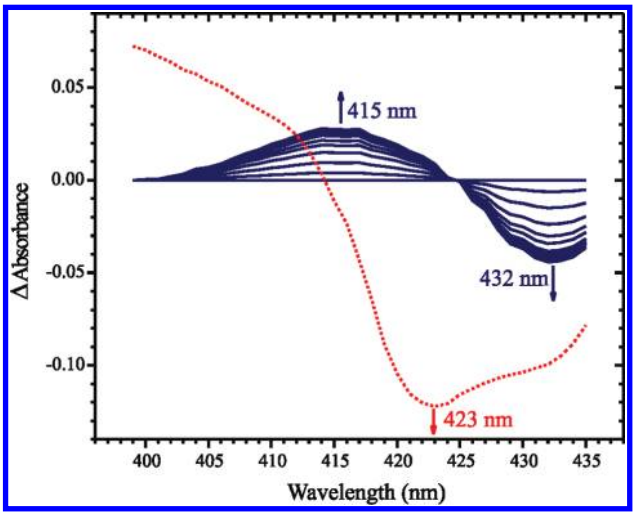

FIGURE 5: Spectral changes (blue traces) observed when a solution initially containing 235 μM $Ru(NH_3)_6^{2+}$, 1 μM $Ru(NH_3)_6^{3+}$, 10 nM HAO, 1.23 μM C_{554}, and 910 μM NH_2OH was allowed to react. Spectra were recorded every 30 s. The red trace is the spectral change expected for oxidation of C_{554}.

Scheme 1

$$Ru(NH_3)_6^{3+} + e^- \rightleftharpoons Ru(NH_3)_6^{2+} \qquad E^0 = -0.024\text{V}$$

$$4Ru(NH_3)_6^{3+} + NH_2OH + H_2O \rightleftharpoons 4Ru(NH_3)_6^{2+} + NO_2^- + 5H^+ \qquad E^0_{cell} = -0.092\text{ V}$$

$$3Ru(NH_3)_6^{3+} + NH_2OH \rightleftharpoons 3Ru(NH_3)_6^{2+} + NO + 3H^+ \qquad E^0_{cell} = 0.003\text{ V}$$

$$2Ru(NH_3)_6^{2+} + NH_2OH \rightleftharpoons Ru(NH_3)_6^{3+} + NH_4^+ + H_2O \qquad E^0_{cell} = 0.91\text{ V}$$

Table 1: Kinetic Parameters Obtained for the Reactions Studied Here

parameter	value	reaction governed
K_{m1}	$(7.6 \pm 0.9) \times 10^{-3}$ M	$NO_2^- + 6MV_{red} + 8H^+ \xrightarrow{HAO} NH_4^+ + 6MV_{ox} + 2H_2O$
k_{cat1}	6.8 ± 0.3 e^-/s	
K_{m2}	$(6.8 \pm 0.2) \times 10^{-3}$ M	$NH_2OH + 2MV_{red} + 3H^+ \xrightarrow{HAO} NH_4^+ + 2MV_{ox} + H_2O$
k_{cat2}	245 ± 3 e^-/s	
K_{m3}	$(5.2 \pm 0.8) \times 10^{-6}$ M	$NH_2OH + 3Ru(NH_3)_6^{3+} \xrightarrow{HAO} NO + 3Ru(NH_3)_6^{2+} + 3H^+$
k_{cat3}	98 ± 3 NO/s	

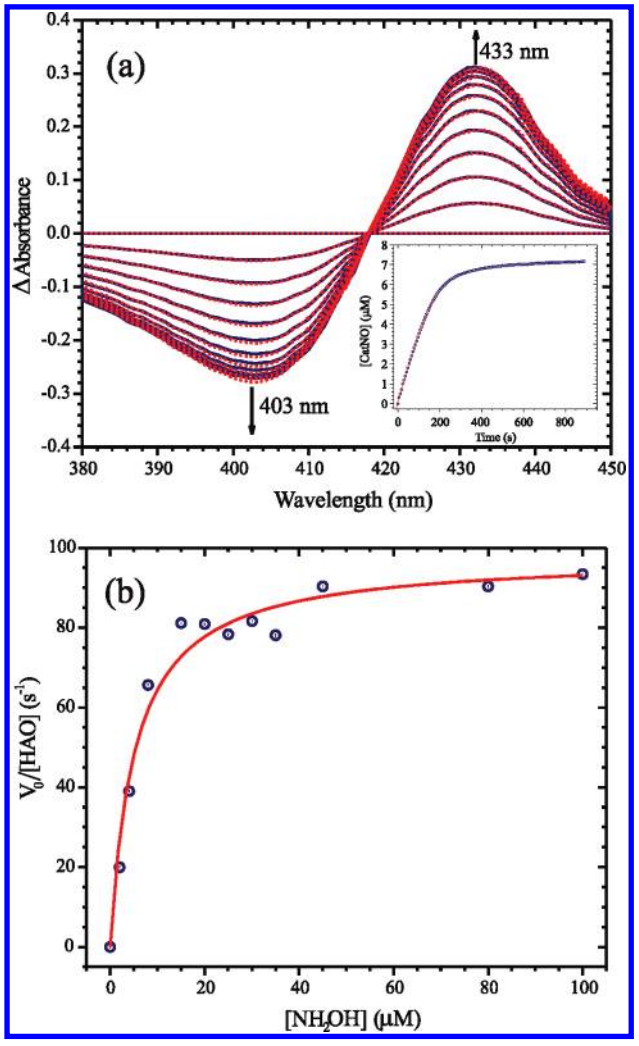

FIGURE 6: (a) Spectral changes (blue traces) observed when a solution initially containing 200 μM $Ru(NH_3)_6^{3+}$, 0.43 nM HAO, 8 μM Cat, and 100 μM NH_2OH was allowed to react. Spectra were recorded every 30 s. Red traces are calculated CatNO − Cat difference spectra obtained from least-squares fitting of the experimental spectra using eq 1. The inset shows changes in CatNO concentration as a function of time. (b) Initial rates of HAO-catalyzed NH_2OH oxidation by $Ru(NH_3)_6^{3+}$ (V_0 = d[CatNO]/dt at time zero) as a function of $[NH_2OH]_0$; V_0/[HAO] is plotted on the abscissa to allow for variation of [HAO] between experiments. The red curve is the least-squares fit to eq 2; the values of the fit parameters, k_{cat3} and K_{m3}, are listed in Table 1.

rate of NO generation. By contrast, in the experiment with C_{554} described above, the appearance of $C_{554}NO$ reflected the rate of C_{554} nitrosylation. Note that we avoided using Cat in experiments designed to study HAO's reductase activity, because Cat itself was found to have significant MV_{red}−NH_2OH oxidoreductase activity (see the Supporting Information), and we have not yet ruled out the possibility that it also has $Ru(NH_3)_6^{2+}$−NH_2OH oxidoreductase activity.

Figure 6a shows the results of an experiment initiated via addition of NH_2OH to a test solution already containing $Ru(NH_3)_6^{3+}$, HAO, and Cat. The concentrations of the reagents after NH_2OH addition were as follows: 200 μM $Ru(NH_3)_6^{2+}$, 0.43 nM HAO, 8 μM Cat, and 100 μM NH_2OH. Analysis of the difference spectra by SVD shows that there is only one component, which can be attributed to Cat nitrosylation. The dashed red lines in Figure 6a represent the least-squares fits to the data, using the independently obtained $\varepsilon_{Cat} - \varepsilon_{CatNO}$ ($\Delta\varepsilon_{Cat}$) difference

Scheme 2: Disproportionation of NH_2OH To Give NH_4^+ and NO[a]

$$5NH_2OH + 3H^+ \longrightarrow 3NH_4^+ + 2NO + 3H_2O$$

[a]Other disproportionation schemes are also possible, as described in ref *30*.

Scheme 3: Ammonia Assay Reaction and Associated Half-Reactions

$$\alpha\text{-KG} + NH_4^+ + 2e^- \longrightarrow \text{Glu} + H_2O$$
$$NADH \longrightarrow NAD^+ + H^+ + 2e^-$$
$$\alpha\text{-KG} + NH_4^+ + NADH \xrightarrow{GDH} \text{Glu} + H_2O + NAD^+ + H^+ \quad \text{net reaction}$$

spectrum. The inset in Figure 6a shows how the CatNO concentration varies as a function of time. The red curve in the inset represents a second-order polynomial fit to the early part of the curve. The initial rate was calculated as the first derivative of the polynomial fit. Figure 6b shows how the initial rate changed when the experiment depicted in Figure 6a was repeated with different NH_2OH initial concentrations. The initial rate of NH_2OH oxidation is seen to exhibit a hyperbolic dependence on NH_2OH concentration; least-squares fitting to the experimental data (red trace in Figure 6b) yields the following parameters: $k_{cat3} = 98 \pm 3\ s^{-1}$, and $K_{m3} = 5.2 \pm 0.8\ \mu$M (Table 1). The k_{cat3} value is comparable to the k_{cat} reported in the literature for HAO-catalyzed oxidation of NH_2OH by phenazine methosulfate ($k_{cat} = 120\ s^{-1}$, and $K_m = 3.6\ \mu$M) (*26*, *27*), while the K_{m3} value is very close to the NH_2OH concentration-dependent K_m value previously reported for HAO-catalyzed oxidation of NH_2OH by cytochrome *c* ($K_m = 3.6\ \mu$M) (*28*).

HAO-Catalyzed Disproportionation of NH_2OH. Inspection of the Frost diagram for nitrogen (Figure 2a) shows that NH_2OH is susceptible to disproportionation into NH_4^+ and NO, according to the reaction of Scheme 2 (*11*). We previously noted that the architecture of HAO (*4*), which allows facile electron transfer between active sites on different subunits of the trimeric enzyme, could in principle make HAO an ideal disproportionation catalyst (*3*). We have now tested this hypothesis directly in two ways.

In one series of experiments, we used the CatNO assay described above. In a solution buffered at pH 7.4, containing 8 μM Cat, 5−10 nM HAO, and 2.5−100 μM NH_2OH, but no added electron acceptor other than NH_2OH, CatNO production was still observed, though at a rate ~60 times lower than that observed when NH_2OH was oxidized by Ru^{III} (see the Supporting Information). No CatNO was generated in the absence of HAO, under otherwise identical conditions. These data suggest that HAO might indeed be catalyzing NH_2OH disproportionation. In a second series of experiments, we used the well-known ammonia assay shown in Scheme 3 (*29*, *30*) to test for NH_4^+ production, under conditions comparable to those described above in the test for CatNO formation. In this assay, glutamate dehydrogenase (GDH) catalyzes the addition of ammonia to α-ketoglutarate (α-KG), which is coupled to NADH oxidation. The assay follows the UV−vis absorbance change at 340 nm due to NADH oxidation (*29*, *30*). Assay results are provided as Supporting Information. In these experiments, we found no significant NH_4^+ production, and hence no convincing evidence of HAO-catalyzed disproportionation to NH_4^+ and NO.

Two mechanisms other than HAO-catalyzed NH_2OH disproportionation could account for the production of CatNO in the

Scheme 4: Summary of HAO's Reductase Properties in the Presence of MV_{red}

$$NO_2^- + MV_{red} + 2H^+ \longrightarrow NO + MV_{ox} + H_2O$$
$$NO + 3MV_{red} + 3H^+ \longrightarrow NH_2OH + 3MV_{ox}$$
$$NH_2OH + 2MV_{red} + 3H^+ \longrightarrow NH_4^+ + 2MV_{ox} + H_2O$$

experiments described above. First, it is possible that trace oxygen, and not NH_2OH, was acting as the electron acceptor in these reactions. Second, it may be that disproportionation does occur, but that the reductive phase is conducted by Cat rather than by HAO. As mentioned earlier, Cat can be an effective NH_2OH reductase in its own right (Supporting Information). Given these two possibilities, and the convincing lack of NH_4^+ formation revealed by the ammonia assay, we conclude that HAO does not catalyze NH_2OH disproportionation, despite the favorable thermodynamics, and the apparent opportunity presented by the HAO architecture.

DISCUSSION

HAO's Reductase Activity. Earlier, we showed that, given a sufficiently potent reducing agent such as MV_{red}, HAO is an excellent NO or NH_2OH reductase (*3*). Herein, we have extended the earlier work to show that HAO is also a competent MV_{red}–NO_2^- oxidoreductase, though the reduction of NO_2^- is several orders of magnitude slower than the subsequent reductions of NO and NH_2OH, at comparable substrate concentrations. Thus, HAO mimics ccNiR in the presence of MV_{red}, in its capacity to reduce NO_2^- all the way to NH_4^+ (Scheme 4).

Having demonstrated HAO's reductase activities in the presence of MV_{red}, we find its lack of hydroxylamine reductase activity, either in the presence of $Ru(NH_3)^{2+}$ or in disproportionation, much more intriguing. Why should HAO-catalyzed NH_2OH reduction by the weaker reducing agents be so much less effective than reduction by MV_{red}? Thermodynamically, there is no reason (as seen in Figure 2a), so we must look for a mechanistic one. One factor that probably plays a role is that, under the conditions used for the MV_{red} experiments (MV_{tot} = 300 μM, and MV_{red} = 40 μM), the P_{460} active site of HAO will be reduced, whereas in the presence of the weaker reductants $Ru(NH_3)^{2+}$ and NH_2OH, it will be oxidized (*31*). Reduction of NH_2OH might well occur faster at a reduced Fe than at an oxidized one. In this regard, it is worth noting that the reported active site midpoint potential of ccNiR from *Escherichia coli* has a substantially higher value than that of HAO: −107 mV (*9*) versus −260 mV (*31*) at pH 7. This means that the ccNiR active site will be mostly in the reduced state during physiological turnover, whereas the HAO active site will be oxidized.

We have independently tested the effect of heme oxidation state on NH_2OH reductase activity by comparing the MV_{red}–NH_2OH oxidoreductase activity of myoglobin (Mb) with that of Cat (see the Supporting Information). Under the reaction conditions, the heme active site of Mb is in the Fe^{II} state, whereas that of Cat remains in the Fe^{III} state. In agreement with our prediction, Mb was found to have a k_{cat} 300 times greater than that of Cat for NH_2OH reduction by MV_{red}. Curiously though, the k_{cat} value for Cat (147 s^{-1}) was comparable to the k_{cat2} for HAO (245 s^{-1}), even though Cat remains oxidized in the presence of MV_{red}. Moreover, the k_{cat} of 45000 s^{-1} for Mb was 2 orders of magnitude greater than that of either HAO or Cat (see the Supporting Information). Thus, even in the presence of MV_{red}, HAO is an ineffective NH_2OH reductase compared to Mb, and only marginally better than Cat.

Scheme 5: A Mechanistic Outline for Explaining the Observed Difference in Values between K_{m2} and K_{m3}[a]

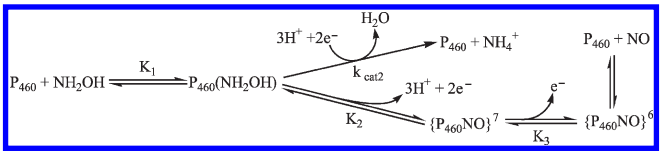

[a]Under strongly reducing conditions, $K_{m2}^{-1} = K_1 = 150$, whereas under normal physiological conditions, $K_{m3}^{-1} = (K_1K_2$ or $K_1K_2K_3) = 1.9 \times 10^5$. Active site Fe–NO fragments are each represented in terms of two resonance structures, and of the corresponding Enemark–Feltham description, $\{FeNO\}^n$. In this notation, the superscript n is the sum of the d electrons that would be counted on Fe if the ligand were actually NO, and the π^* electron from the NO (*32*). Note that "P_{460}" is used in place of "Fe" in the notation, to emphasize that it is the P_{460} heme that is nitrosylated.

In addition to the role that the P_{460} oxidation state may play, Scheme 5 suggests a second mechanism to account for HAO's poor or absent NH_2OH reductase activity when $Ru(NH_3)^{2+}$ or NH_2OH is used as the e^- donor. In this scenario, NH_2OH binds weakly to the P_{460} active site in an equilibrium governed by K_1. Except under strongly reducing conditions, most of the NH_2OH that does bind is then oxidized to yield $\{P_{460}NO\}^7$ or $\{P_{460}NO\}^6$ via the rapid equilibria governed by K_2 and K_3 (see ref *32* and Scheme 5 for a description of the $\{FeNO\}^n$ formalism). Thus, NH_2OH reduction is minimized by minimizing the concentration of the critical enzyme-bound intermediate, $P_{460}(NH_2OH)$. The mechanism of Scheme 5 is consistent with the kinetic data reported in this paper, and data previously reported by other authors. Hooper and co-workers showed in stopped-flow investigations that reduction of the HAO *c* hemes by NH_2OH occurs on the millisecond time scale at 2 °C and is too fast to measure at room temperature (*26*). This would be fast enough to establish the rapid equilibria that we propose. From our current studies, the most striking observation is the ~10^3-fold difference between the K_m value for NH_2OH reduction by MV_{red} ($K_{m2} = 6.8 \times 10^{-3}$ M) and that for its oxidation by $Ru(NH_3)_6^{3+}$ ($K_{m3} = 5.2 \times 10^{-6}$ M), at the HAO active site (Table 1). Such a large difference in values immediately rules out the naive Michaelis–Menten interpretation of a single K_m governing the binding of NH_2OH to P_{460} under all circumstances. We propose that K_{m2} does indeed govern the binding of NH_2OH to P_{460}, so that K_1 in Scheme 5 has a numerical value of 150 ($= K_{m2}^{-1}$). In the presence of MV_{red}, even the P_{460} active site is reduced, so in situ oxidation of NH_2OH cannot occur. Thus, the intermediate $P_{460}(NH_2OH)$ accumulates, allowing the bound NH_2OH to be reduced. In the presence of a less potent reducing agent such as $Ru(NH_3)_6^{2+}$ or NH_2OH itself, the equilibrium among intermediates $P_{460}(NH_2OH)$, $\{P_{460}NO\}^7$, and possibly $\{P_{460}NO\}^6$ will be rapidly established and lie far to the right. The K_m value (K_{m3}) should now reflect the product of equilibrium constants, K_1K_2 or $K_1K_2K_3$, instead of the single constant K_1. On the basis of the value of K_{m3} [5.2×10^{-6} M (Table 1)], product K_1K_2 or $K_1K_2K_3$ would have a numerical value of 1.9×10^5 ($= K_{m3}^{-1}$). From this value and the value of K_1 calculated above (assuming for the moment that K_1 is unaffected by the P_{460} oxidation state), we can estimate a value of 1300 for the equilibrium constant K_2 or K_2K_3 that governs the oxidation of $P_{460}(NH_2OH)$ to $\{P_{460}NO\}^7$ or $\{P_{460}NO\}^6$ by $Ru(NH_3)_6^{3+}$ at pH 7.4. According to Scheme 5, this equilibrium constant should

depend on pH; though we have not yet checked this, HAO activity and the reactivity of the P_{460} active site are both known to be strongly pH-dependent (*26*, *28*). Finally, from the predicted equilibrium constant for oxidation of $P_{460}(NH_2OH)$ to $\{P_{460}NO\}^7$ or $\{P_{460}NO\}^6$ by $Ru(NH_3)_6^{3+}$, we can estimate the midpoint potential for reduction of $\{P_{460}NO\}^7$ or $\{P_{460}NO\}^6$ to $P_{460}(NH_2OH)$ to be −0.116 V.

Note that the mechanistic explanation in Scheme 5 does not preclude a role for the P_{460} oxidation state in modulating HAO's NH_2OH reductase activity, as suggested earlier. Within Scheme 5, the earlier explanation simply means that k_{cat2} has a higher value when P_{460} is reduced. Similarly, the value of K_1 need not be the same for ferrous and ferric P_{460}, in which case our analysis above over- or underestimates the value of K_2 or K_2K_3. Nevertheless, in Scheme 5, such variations in k_{cat2} and K_1 with oxidation state would be contributing factors instead of the complete explanation for HAO's poor reductase activity at higher potentials.

NO Trapping Experiments. The experiments with Cat demonstrate that HAO-catalyzed NH_2OH oxidation by $Ru(NH_3)_6^{3+}$ is as fast as its aerobic oxidation to NO_2^- by phenazine methosulfate (*26*, *27*) and results in release of free NO. The generation of NO instead of NO_2^- during HAO-catalyzed anaerobic oxidation of NH_2OH was first conclusively demonstrated by Hooper and Terry 30 years ago, but not studied in detail (*33*). Figure 1 and Scheme 5 show how NO could be released from HAO instead of NO_2^-, while Scheme 1 (and Figure 2a) shows how thermodynamics at pH 7 favor production of NO over NO_2^- when $Ru(NH_3)_6^{3+}$ is the sole electron acceptor. Studies with synthetic Fe porphyrin complexes and simple heme proteins show that in general NO is bound tightly within $\{P_{460}NO\}^7$ species but is labile as $\{P_{460}NO\}^6$ (*34*, *35*). The NO-generating mechanism of Scheme 5 is consistent with these studies. On the other hand, in a recent paper Hendrich et al. provided clear spectroscopic evidence that when fully oxidized HAO is exposed to 1 atm of NO, the NO binds strongly to the P_{460} active site, forming a long-lived $\{FeNO\}^6$ intermediate that can be broken apart only by photolysis (*36*). Because our results and the earlier ones of Hooper and Terry (*33*) unambiguously show that NO is released from HAO under catalytic conditions, some process must trap the NO at the P_{460} active site under the conditions employed by Hendrich et al. One possible explanation is that, given enough time, HAO in the presence of NO undergoes a conformational change that traps the NO at the P_{460} active site. This is how NO is tightly bound in nitrophorins, which also have the binding site Fe in the +3 state (*37*). We are currently investigating this hypothesis in our laboratory.

Summary. When we first reported on the ability of HAO to act as a reductase (*3*), we emphasized the possible physiological roles that such reductase activity might have. Our latest results have caused us to turn our emphasis around: it appears that though HAO can be forced to act as a reductase under extreme conditions, the enzyme is in fact exquisitely tuned to minimize such activity under more physiologically relevant conditions. Such a view is supported by our studies with Mb and Cat (see the Supporting Information), which suggest that no special requirements are needed to obtain NH_2OH reductase activity at Fe centers. It is also consistent with our observation that HAO does not catalyze NH_2OH disproportionation, even though its architecture could in principle make it an ideal disproportionation catalyst. It is easy to see why HAO should have evolved to discourage NH_2OH reductase activity. As shown in Figure 2b, AMO-catalyzed oxidation of NH_4^+ to NH_2OH in *Nitrosomonas europaeae* is endoergic, even when coupled to reduction of oxygen. Thus, *N. europaeae* derive all the energy for their growth from the HAO-catalyzed oxidation of NH_2OH. HAO-catalyzed reduction of NH_2OH back to NH_4^+ would short-circuit the energy-generating process and waste a large amount of the needed energy. We propose that NH_2OH reductase activity in HAO is discouraged by keeping the P_{460} active site oxidized under physiological conditions and by minimizing the accumulation of a $P_{460}(NH_2OH)$ intermediate, which would be necessary for efficient reductase activity. We further propose that thermodynamically and kinetically facile oxidation of the $P_{460}(NH_2OH)$ intermediate to $\{P_{460}NO\}^7$ or $\{P_{460}NO\}^6$ plays an important role in minimizing its accumulation, as shown in Scheme 5. How the unique structural features of the HAO active site contribute to the proposed mechanisms is at this point still an open question, and one of intense interest to our laboratory. What is clear is that for all its superficial similarity to ccNiR, HAO has evolved to be just the right tool for the job of NH_2OH oxidation, even under conditions that thermodynamically favor its reduction to ammonia instead.

SUPPORTING INFORMATION AVAILABLE

Myoglobin-mediated reduction of NH_2OH by MV_{red} and plot of V_0/[Mb] versus [NH_2OH]; catalase-mediated reduction of NH_2OH by MV_{red} and plot of V_0/[Cat] versus [NH_2OH]; results of tests for HAO-mediated disproportionation of NH_2OH (test for CatNO formation and test for NH_4^+ formation). This material is available free of charge via the Internet at http://pubs.acs.org.

REFERENCES

1. Schmidt, I., Steenbakkers, P. J. M., op den Camp, H. J. M., Schmidt, K., and Jetten, M. S. M. (2004) Physiologic and proteomic evidence for a role of nitric oxide in biofilm formation by *Nitrosomonas europaea* and other ammonia oxidizers. *J. Bacteriol. 186*, 2781–2788.
2. Ehrlich, H. L. (2002) Geomicrobiology, 4th ed., Marcel Dekker, Inc., New York.
3. Kostera, J., Youngblut, M. D., Slosarczyk, J. M., and Pacheco, A. A. (2008) Kinetic and product distribution analysis of NO reductase activity in *Nitrosomonas europaea* hydroxylamine oxidoreductase. *J. Biol. Inorg. Chem. 13*, 1073–1083.
4. Igarashi, N., Moriyama, H., Fujiwara, T., Fukumori, Y., and Tanaka, N. (1997) The 2.8 angstrom structure of hydroxylamine oxidoreductase from a nitrifying chemoautotrophic bacterium, *Nitrosomonas europaea*. *Nat. Struct. Biol. 4*, 276–284.
5. Arciero, D. M., and Hooper, A. B. (1993) Hydroxylamine Oxidoreductase from *Nitrosomonas europaea* Is a Multimer of an Octa-Heme Subunit. *J. Biol. Chem. 268*, 14645–14654.
6. Kurnikov, I. V., Ratner, M. A., and Pacheco, A. A. (2005) Redox equilibria in hydroxylamine oxidoreductase. Electrostatic control of electron redistribution in multielectron oxidative processes. *Biochemistry 44*, 1856–1863.
7. Einsle, O., Messerschmidt, A., Stach, P., Bourenkov, G. P., Bartunik, H. D., Huber, R., and Kroneck, P. M. H. (1999) Structure of cytochrome c nitrite reductase. *Nature 400*, 476–480.
8. Einsle, O., Stach, P., Messerschmidt, A., Simon, J., Kroger, A., Huber, R., and Kroneck, P. M. H. (2000) Cytochrome c nitrite reductase from *Wolinella succinogenes*: Structure at 1.6 angstrom resolution, inhibitor binding, and heme-packing motifs. *J. Biol. Chem. 275*, 39608–39616.
9. Bamford, V. A., Angove, H. C., Seward, H. E., Thomson, A. J., Cole, J. A., Butt, J. N., Hemmings, A. M., and Richardson, D. J. (2002) Structure and spectroscopy of the periplasmic cytochrome c nitrite reductase from *Escherichia coli*. *Biochemistry 41*, 2921–2931.
10. Cunha, C. A., Macieira, S., Dias, J. M., Almeida, G., Goncalves, L. L., Costa, C., Lampreia, J., Huber, R., Moura, J. J. G., Moura, I., and Romao, M. J. (2003) Cytochrome c nitrite reductase from *Desulfovibrio desulfuricans* ATCC 27774: The relevance of the two calcium sites in the structure of the catalytic subunit (NrfA). *J. Biol. Chem. 278*, 17455–17465.

11. Atkins, P., Overton, T., Rourke, J., Weller, M., Armstrong, F., and Hagerman, M. (2010) Shriver and Atkins' Inorganic Chemistry, 5th ed., pp 147−178, W. H. Freeman and Co., New York.
12. Koppenol, W. H., Moreno, J. J., Pryor, W. A., Ischiropoulos, H., and Beckman, J. S. (1992) Peroxynitrite, a Cloaked Oxidant Formed by Nitric-Oxide and Superoxide. *Chem. Res. Toxicol. 5*, 834–842.
13. Cabail, M. Z., and Pacheco, A. A. (2003) Selective One-Electron Reduction of *Nitrosomonas europaea* Hydroxylamine Oxidoreductase with Nitric Oxide. *Inorg. Chem. 42*, 270–272.
14. Arciero, D. M., Balny, C., and Hooper, A. B. (1991) Spectroscopic and Rapid Kinetic Studies of Reduction of Cytochrome-C554 by Hydroxylamine Oxidoreductase from *Nitrosomonas europaea*. *Biochemistry 30*, 11466–11472.
15. Press, W. H., Teukolsky, S. A., Vetterling, W. T., and Flannery, B. P. (1992) The Art of Scientific Computing, 2nd edition, Cambridge University Press, Cambridge, U.K.
16. Strang, G. (1988) Linear Algebra and Its Applications, 3rd ed., Harcourt Brace Jovanivich, Inc., San Diego.
17. Vlasits, J., Jakopitsch, C., Schwanninger, M., Holubar, P., and Obinger, C. (2007) Hydrogen peroxide oxidation by catalase-peroxidase follows a non-scrambling mechanism. *FEBS Lett. 581*, 320–324.
18. Drago, R. S., and Paulik, F. E. (1960) The Reaction of Nitrogen(II) Oxide with Diethylamine. *J. Am. Chem. Soc. 82*, 96–98.
19. Maragos, C. M., Morley, D., Wink, D. A., Dunams, T. M., Saavedra, J. E., Hoffman, A., Bove, A. A., Isaac, L., Hrabie, J. A., and Keefer, L. K. (1991) Complexes of NO with Nucleophiles as Agents for the Controlled Biological Release of Nitric Oxide: Vasorelaxant Effects. *J. Med. Chem. 34*, 3242–3247.
20. Codd, R., Astashkin, A. V., Pacheco, A., Raitsimring, A. M., and Enemark, J. H. (2002) Pulsed ELDOR spectroscopy of the Mo(V)/Fe(III) state of sulfite oxidase prepared by one-electron reduction with Ti(III) citrate. *J. Biol. Inorg. Chem. 7*, 338–350.
21. Andersson, K. K., Lipscomb, J. D., Valentine, M., Munck, E., and Hooper, A. B. (1986) Tetraheme Cytochrome c-554 from *Nitrosomonas europaea*. *J. Biol. Chem. 261*, 1126–1138.
22. Kostera, J. (2010) Hydroxylamine oxidase: Mechanistic insights from running the enzyme in reverse. Ph.D. Dissertation, University of Wisconsin, Milwaukee, WI.
23. Whittaker, M., Bergmann, D., Arciero, D., and Hooper, A. B. (2000) Electron transfer during the oxidation of ammonia by the chemolithotrophic bacterium *Nitrosomonas europaea*. *Biochim. Biophys. Acta 1459*, 346–355.
24. Upadhyay, A. K., Petasis, D. T., Arciero, D. M., Hooper, A. B., and Hendrich, M. P. (2003) Spectroscopic characterization and assignment of reduction potentials in the tetraheme cytochrome c_{554} from *Nitrosomonas europaea*. *J. Am. Chem. Soc. 125*, 1738–1747.
25. Upadhyay, A. K., Hooper, A. B., and Hendrich, M. P. (2006) NO reductase activity of the tetraheme cytochrome c_{554} of *Nitrosomonas europaea*. *J. Am. Chem. Soc. 128*, 4330–4337.
26. Hooper, A. B., Tran, V. M., and Balny, C. (1984) Kinetics of reduction by substrate or dithionite and heme-heme electron transfer in the multiheme hydroxylamine oxidoreductase. *Eur. J. Biochem. 141*, 565–571.
27. Hooper, A. B., Maxwell, P. C., and Terry, K. R. (1978) Hydroxylamine oxidoreductase from *Nitrosomonas*: Absorption spectra and content of heme and metal. *Biochemistry 17*, 2984–2989.
28. Hooper, A. B., and Nason, A. J. (1965) Characterization of hydroxylamine-cytochrome *c* reductase from the chemoautotrohs *Nitrosomonas europaea* and *Nitrosocystis oceanus*. *J. Biol. Chem. 240*, 4044–4057.
29. Bergmeyer, H. U., and Beutler, H. O. (1985) in Methods of Enzymatic Analysis (Bergmeyer, H. U., Ed.) Vol. 8, pp 454−461, Academic Press, New York.
30. Pacheco, A. A., McGarry, J. M., Kostera, J., and Corona, A. (2010) Techniques for Investigating Hydroxylamine Disproportionation by Hydroxylamine Oxidoreductases. In Methods in Enzymology (Klotz, M. G., Ed.) Academic Press, Inc., San Diego (in press).
31. Collins, M. J., Arciero, D. M., and Hooper, A. B. (1993) Optical Spectropotentiometric Resolution of the Hemes of Hydroxylamine Oxidoreductase: Heme Quantitation and pH-Dependence of E_m. *J. Biol. Chem. 268*, 14655–14662.
32. Enemark, J. H., and Feltham, R. D. (1974) Principles of Structure, Bonding and Reactivity for Metal Nitrosyl Complexes. *Coord. Chem. Rev. 13*, 339–406.
33. Hooper, A. B., and Terry, K. R. (1979) Hydroxylamine oxidoreductase of nitrosomonas: Production of nitric oxide from hydroxylamine. *Biochim. Biophys. Acta 571*, 12–20.
34. Ellison, M. K., and Scheidt, W. R. (1999) Synthesis, molecular structures, and properties of six-coordinate $[Fe(OEP)(L)(NO)]^+$ derivatives: Elusive nitrosyl ferric porphyrins. *J. Am. Chem. Soc. 121*, 5210–5219.
35. Ford, P. C., and Lorkovic, I. M. (2002) Mechanistic aspects of the reactions of nitric oxide with transition-metal complexes. *Chem. Rev. 102*, 993–1017.
36. Hendrich, M. P., Upadhyay, A. K., Riga, J., Arciero, D. M., and Hooper, A. B. (2002) Spectroscopic characterization of the NO adduct of hydroxylamine oxidoreductase. *Biochemistry 41*, 4603–4611.
37. Andersen, J. F., Ding, X. D., Balfour, C., Shokhireva, T. K., Champagne, D. E., Walker, F. A., and Montfort, W. R. (2000) Kinetics and equilibria in ligand binding by nitrophorins 1−4: Evidence for stabilization of a nitric oxide-ferriheme complex through a ligand-induced conformational trap. *Biochemistry 39*, 10118–10131.